Received: 26 July 2023 | Revised: 4 December 2023 | Accepted: 22 January 2024

Healthcare Technology Letters

DOI: 10.1049/htl2.12075

The Institution of Engineering and Technology WILEY

LETTER

Contactless and short-range vital signs detection with doppler radar millimetre-wave (76–81 GHz) sensing firmware

Pi-Yun Chen[1] | **Hsu-Yung Lin**[1] | **Zi-Heng Zhong**[1] | **Neng-Sheng Pai**[1] | **Chien-Ming Li**[2] | **Chia-Hung Lin**[1]

[1]Department of Electrical Engineering, National Chin-Yi University of Technology, Taichung City, Taiwan

[2]Department of Medicine of Chi Mei Medical Center, Chien-Ming Li is with the Division of Infectious Diseases, Tainan City, Taiwan

Correspondence
Pi-Yun Chen and Chia-Hung Lin, Department of Electrical Engineering, National Chin-Yi University of Technology, Taichung City, Taiwan.
Email: chenby@ncut.edu.tw and eechl53@gmail.com

Funding information
National Science and Technology Council (NSTC), Grant/Award Number: NSTC 111-2221-E-167-034; National Chin-Yi University of Technology, Grant/Award Number: NCUT 23-R-CE-009

Abstract

Vital signs such as heart rate (HR) and respiration rate (RR) are essential physiological parameters that are routinely used to monitor human health and bodily functions. They can be continuously monitored through contact or contactless measurements performed in the home or a hospital. In this study, a contactless Doppler radar W-band sensing system was used for short-range, contactless vital sign estimation. Frequency-modulated continuous wave (FMCW) measurements were performed to reduce the influence of a patient's micromotion. Sensing software was developed that can process the received chirps to filter and extract heartbeat and breathing rhythm signals. The proposed contactless sensing system eliminates the need for the contact electrodes, electric patches, photoelectric sensors, and conductive wires used in typical physiological sensing methods. The system operates at 76–81 GHz in FMCW mode and can detect objects on the basis of changes in frequency and phase. The obtained signals are used to precisely monitor a patient's HR and RR with minimal noise interference. In a laboratory setting, the heartbeats and breathing rhythm signals of healthy young participants were measured, and their HR and RR were estimated through frequency- and time-domain analyses. The experimental results confirmed the feasibility of the proposed W-band mm-wave radar for contactless and short-range continuous detection of human vital signs.

1 | INTRODUCTION

Vital sign monitoring can provide valuable information for the early detection of diseases such as heart disease and cardiovascular-related conditions. In particular, electrocardiography (ECG) and photoplethysmography (PPG) can measure heart rate (HR) and monitor cardiac activity. In ECG measurements, three leads (leads I, II, and III) are used to measure electrical activity signals from the atria to the ventricles in the heart. An ECG reading has the form of a waveform, including P, QRS complex, and T waves. These waveforms can be used to identify cardiac arrhythmia, heart conduction disorders, coronary ischemia, myocardial infarction, and atrial fibrillation. Regular contractions and relaxations of the atria and ventricles can drive blood flow from the heart through the pulmonary and systemic circulation systems. Each heartbeat triggers a blood pressure wave that passes through the blood vessels, causing regular pulsation as the vessels contract and expand. These pulsations can be measured using PPG, which can thus detect physiological parameters such as HR, HR variability (HRV), oxygen saturation (SPO_2), and respiration rate (RR) [1–6].

To perform ECG measurements, contact electrodes and electric patches must be placed on the human body, including on the upper and lower limbs and chest [6]. These contact sensors are attached to the skin to perform up to 12-lead measurements between any two sensors, enabling continuous monitoring of the heart's electrical activity. However, measurement quality can be degraded by environmental factors or subject motion; hence, patient movement must be restricted. PPG measurements are performed using a photoemitter and a photodetector in either transmissive or reflective mode [1, 3]. A photoemitter can emit visible green light (510 nm), visible red light (659 nm), or near-infrared (IR) light (800–940 nm); the photodetector then measures changes in the reflected light [1, 3, 7]. In transmissive

mode, the light intensity is 40–60 dB stronger than in reflective mode; however, reflective-mode PPG can be performed for any location on the human body, including the thumbs, fingers, and earlobes. An appropriate wavelength range must be selected to ensure sufficient light transmission and measurement resolution. PPG with IR light has a broad sensitivity range and sufficient resolution to measure physical changes in blood vessels. Hence, optical sensing methods are increasingly employed in wearable devices, such as wrist-worn fitness trackers, for continuous and long-term physiological monitoring.

Each PPG pulse trails an ECG signal; hence, ECG and PPG can be combined to measure the pulse transit time and blood velocity. These measurements can be input into a characteristic equation for estimating systolic and diastolic blood pressure for continuous blood pressure monitoring. Combining these measurements is a non-invasive method of estimating physiological parameters such as the stiffness index (SI) or reflection index (RI) [7, 8] and of evaluating the risk of cardiovascular disease or arteriosclerosis. The advantages and limitations of ECG and PPG measurements are as follows:

- ECG measurements: Commercial ECG methods are used as a first-line tool for the early detection of heart disease. However, ECG signals are faint (on the order of millivolts) and have a frequency of less than a few hundred hertz; hence, they are susceptible to interference from noise due to power lines (50 or 60 Hz), impedance from skin contact, and high-frequency electromagnetic signals. This noise can be eliminated using digital band-rejection filters (50 or 60 Hz), digital baseline-drift filters (5–12 Hz), and digital bandpass filters (1–30 Hz) [9, 10]. In practical applications, ECG is a time-consuming method for monitoring a patient in a hospital environment and requires the interpretation of data by medical staff.
- PPG measurements: Noise that interferes with optical PPG measurements can be caused by ambient light, sweat, and vibrations due to patient motion. Ambient light, such as from fluorescent bulbs, may incur noise attributable to alternating current [11–13]; this noise can be reduced by using digital filters. Wearable PPG sensors can be employed during dynamic activities but are susceptible to interference attributable to the relative motion of the optical sensor and the skin, resulting in low signal sensitivity. In addition, the frequency of motion vibration can be misinterpreted as the RR and must therefore be compensated for when measurements are being recorded during dynamic activities.

Both ECG and PPG contact measurements require the placement of electrodes or optical sensors on the skin and an external connection to a data processor through signal-conducting wires. Long-term monitoring with such a setup can cause discomfort for patients and limit their movement. Contactless measurements do not cause discomfort or adverse biological monitoring with a mm-wave sensing system; (b) detection of frequency displacements (f_r) produced by a stationary object; and (c) detection of frequency displacements produced by dynamic object reactions, such as infection, skin irritation, and allergic reactions. Clinically, contactless measurements are employed for patients with special treatment requirements, such as patients with severe burns in the intensive care unit (ICU), with a novel infectious disease (such as COVID-19), in the neonatal ICU (NICU) [2, 14–16], or with severe wounds and at high risk of infection. The continuous monitoring of vital signs is essential for obtaining estimations of a patient's HR, RR, and SpO_2 to monitor for hypoxia, heart health, autonomic nervous system function (as indicated by HRV), and systemic inflammatory response or autoimmune disorders [14, 15]. Contactless monitoring methods can prevent human-to-human transmission of disease and also reduce stress, pain, and damage to the fragile skin of infants and injured adults [2]. Contactless measurements enable long-term and continuous monitoring and do not suffer from the shortcomings of contact methods, such as signal-conducting wires becoming detached.

To make contactless measurements, this study applied Doppler millimetre-wave (mm-wave) radar with frequency-modulated continuous wave (FMCW) technology [16, 17] for vital sign detection (VSD) applications, including HR and RR estimations [5, 18–25]. An overview of the method is presented in Figure 1a. The mm-wave bands of the radar can be segmented into the C-band (4–8 GHz), X-band (8–12.5 GHz), K-band (12.5–40.0 GHz), V-band (40–75 GHz), and W-band (75–110 GHz) [5, 16, 20, 26]; these bands can be measured using the commercial circuit boards and embedded modules shown in Figure 2. Among these mm-wave bands, the 3–30 GHz mm-wave is commonly used in everyday life, and the X-band is a standard range for radar sensing applications in various industries and healthcare. For example, commercial mm-wave circuit boards (TRW-5.8G-B and HB100 Radar) [20] and embedded modules (SW-UWB-M-DEBUG-V2, SW-UWB-M-A2 × 2, and Texas Instruments radar sensor (TI IWR1443BOOST) [5]), as seen in Figure 2, generally operate within specific bands in the 5.8 GHz, 6.5–8.1 GHz, 10.525 GHz, and 76–81 GHz mm-wave ranges. The commercial SW-UWB-M-A2 × 2 radar module, with a lower transmission frequency, offers a broad detection range of 0.5–3.0 m. X-band mm-wave sensors are widely used in commercial and industrial applications, such as theft deterrence, traffic speed detection, automated controls, and VSD [26]. However, widespread usage of this band results in high interference. The K-band is commonly employed for high-discriminant-validity measurements; however, atmospheric attenuation causes it to have a short detection range of less than 1.0 m [20, 23, 24, 27, 28]. The TI mm-wave radar sensor (IWR1443BOOST# or IWR1642BOOST#) [5, 16] is a multi-input, multi-output-capable hardware–software single-chip (two transmitters and four receivers) device that has a development kit and an application programming interface. Therefore it could be used to develop a VSD system. However, this chip is slightly more sensitive to random body motion than 60-GHz systems because of the greater path loss (antenna peak gain of >9 dBi) across the 76–81 GHz frequency band [29, 30]. The bottleneck for data measurements is the sensing range; a radar sensor's accuracy decreases greatly as the sensing range decreases. The maximum measurement

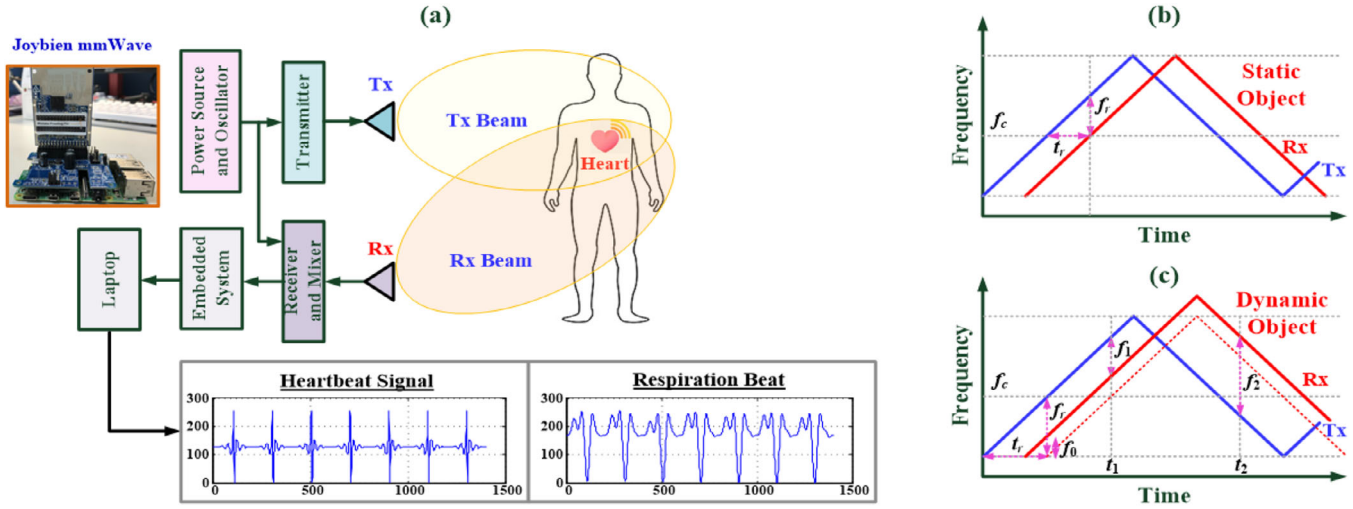

FIGURE 1 Doppler millimetre (mm)-wave radar-based contactless measurement system. (a) Vital signs (HR and RR detection) are continuous.

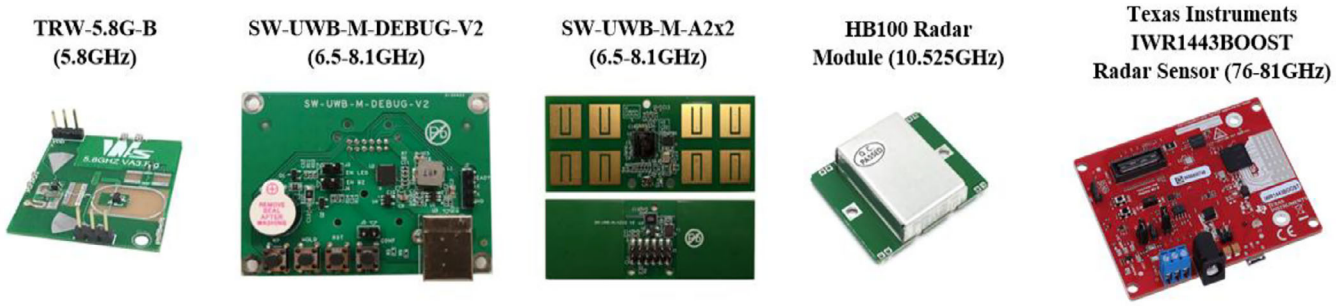

FIGURE 2 Commercial millimetre-wave radar circuit boards and embedded modules.

distance of a sensor being used for HR and RR estimation is approximately 1.2 m (0.6–1.2 m) for standing or walking patients [5, 16].

In this study, we employed a W-band FMCW-based mm-wave (76–81 GHz) sensing system for human VSD. The system is an embedded module comprising a radio frequency transmission circuit, reviver antennas, a power amplifier, a filter system, and a microcontroller. The system preprocesses sensing signals and then transmits them to a laptop for digital data analysis. The distance and direction of measurements can be estimated by analyzing the frequency differences between transmitted and reflected electromagnetic waves. Application of the system to stationary and dynamic object detection is depicted in Figure 1b,c, respectively. Dynamic or stationary objects can be detected and tracked. Doppler mm-wave radar is employed to detect heartbeat and breathing rhythm signals in contactless measurements, and digital filters are used to eliminate interference, such as microdisturbances from the body, background noise, and DC offsets in the system. The phase value of the received chirps is filtered using a bi-quad infinite impulse response (IIR) filter [5, 29] into 0.8–4.0 and 0.1–0.6 Hz components; these represent, respectively, the cardiac and breathing frequency spectra [5, 29]. This method enables the mitigation or complete elimination of interference. In addition, for short-range detection, reducing the radar wavelength can decrease the reception of interference signals, thereby reducing measurement errors in the intermodulation signals. Digital signal processing can also be performed on a laptop to remove unwanted low-frequency and high-frequency signals with a bandpass filter (the Butterworth filter) to yield physiological parameters suitable for estimating HR and RR.

For digital signal analysis, we estimated HR and RR by using frequency-domain and time-domain methods. Regarding the frequency- domain method, the fast Fourier transform (FFT) was first employed to extract characteristic frequencies from the postprocessed signals. Typically, the characteristic frequencies are 1.1–1.3 Hz for heartbeat signals and 0.15–0.40 Hz for breathing rhythm signals [31]. The HR and RR could both be estimated from these specific characteristic frequencies. An adult human typically has a resting HR of 60–70 beats/min and a resting RR of 12–20 breaths/min; both of these increase during exercise. Regarding the time-domain method, the peak detection or endpoint detection algorithm [5, 6, 32] was used to identify the peaks of the heartbeat signals by applying preset threshold values (a peak-to-peak distance threshold and an amplitude threshold) as a benchmark (peak-to-peak interval) for estimating the average R-R interval; the average HR was then computed [5, 6]. The aforementioned digital filters

and signal processing algorithms can all be implemented in Python [17]. Thus, we established a Doppler mm-wave radar with FMCW technology (Figure 1a) that can make contactless, short-range measurements to capture heartbeat and breathing rhythm signals. This setup enabled us to extract characteristic frequencies and parameters to determine HR and RR in both the time and frequency domains. Through experiments, we verified that the data captured by the W-band mm-wave radar can be used for real-time human VSD, thereby demonstrating the accuracy of mm-wave radar for contactless measurements.

2 | METHODOLOGY

2.1 | Principles of contactless mm-wave radar sensing

As seen in Figure 1a, the contactless mm-wave radar used in this study is a 71–86 GHz mm-wave sensing firmware device (76–77 GHz: 14 dB; 77–81 GHz: 15 dB). This HW-SW device consists of a radar mm-wave sensor (Joybien mm-wave IWR1642BOOST single chip), a Raspberry-Pi Hat Board (ARM Cortex-R4F-based radio control system), and Python application software [5, 17, 29]. Utilizing the Doppler effect application, as seen in Figure 1a, an electromagnetic wave is emitted from the transmitter end, Tx, toward a stationary or a dynamic object. The object then reflects the electromagnetic wave back to the receiving end, Rx. The digital signal processor captures and processes the reflected signal, facilitating the estimation of the object's motion, distance, speed, and direction or angle based on frequency and phase changes, as seen in Figure 1b,c, respectively. Currently, three dominant mm-wave radar technologies include: (1) pulse modulation (PM); (2) continuous wave (CW); and (3) frequency modulation (FM) [17–20]. Unmodulated CW radars can detect the Doppler frequency shifts caused by changes in object velocity. The object's distance must be measured with FM, whereas PM can only detect the object's distance. The FMCW method can simultaneously detect both an object's distance and velocity [17, 22–24]. In this study, we employ a Doppler mm-wave radar to perform continuous, contactless, short-range measurement for estimating HR and RR based on frequency differences between the Tx and Rx ends. Figure 1b shows the incident electromagnetic wave striking a stationary object [22–24]. The reflected incident wave exhibits identical waveforms and frequencies. A time delay, t_r, develops between both electromagnetic waves due to the distance, d_0; the distance between the object and the radar can be represented as $d_0 = c \cdot t_r / 2$, with c representing the signal propagation velocity in the air and is given as $c = 3 \times 10^8$ m/s. Let the object's motion signal, $x(t)$, as [20]

$$x(t) = A_0 \cos(2\pi f_0 t + \theta(t)) \tag{1}$$

where A_0 is the signal amplitude and f_0 is the frequency. Given f_T and $\theta(t)$ as the transmitted frequency and phase noise, the reflected signal, $R(t)$, can be represented as [5, 20]

$$\mathrm{R}(t) \approx A_{\mathrm{R}} \cos(2\pi f_{\mathrm{T}} t) - \frac{4\pi d_0}{\lambda_T} - \frac{4\pi x(t)}{\lambda_T} + \theta\left(t - \frac{2d_0}{c}\right) \tag{2}$$

where A_{R} is the amplitude of the reflected signal $R(t)$; $\lambda_T = c / f_T$ is the wavelength; and d_0 is the fixed distance between the object and the stationary radar sensor. Suppose $\theta_0 = 4\pi d_0 / \lambda_T$ be the phase shift and $\Delta\theta(t) = \theta(t) - \theta(t - 2d_0/c)$ be the residual phase noise. With the mixing process, we can obtain the normalized baseband signal, $B(t)$, as follows [5, 20]:

$$\mathrm{B}(t) \approx \cos\left(\theta_0 + \frac{4\pi x(t)}{\lambda_T} + \Delta\theta(t)\right) \tag{3}$$

Considering θ_0 as an odd multiple of $\pi/2$ and $x(t) << \lambda_T$, we can simplify the Equation (3) as

$$B(t) \approx \frac{4\pi x(t)}{\lambda_T} + \Delta\theta(t) \tag{4}$$

Figure 1c shows that if the object is in motion, the electromagnetic wave is reflected by a target moving relative to the radar, and then the reflected electromagnetic wave demonstrates a frequency shift, f_d; the frequency changes of the processed signal can be expressed as "$f_1 = f_r - f_d$" and "$f_2 = f_r + f_D$", respectively. The distance between the radar and the object can be estimated as distance $D = (c / (4 \times f_m \times b)) \times ((f_2 + f_1)/2)$, where frequency, f_m, indicates the modulation frequency, and b represents the maximum change in the modulation frequency. The relative velocity of the dynamic object is $v = (\mathrm{c} / (2 \times f_c)) \times ((f_2 - f_1)/2)$, where frequency, f_c, denotes the centre frequency of the incident electromagnetic wave [22–24], thus enabling detection of the dynamic object's distance and motion velocity.

For the same stationary object, with a displacement of <5 mm and a frequency of <2 Hz, the phase change is constant [5, 29]; thus, $x(t)$ in Equation (4) can be expressed as follows [25]:

$$\mathrm{x}(t) \approx x_b(t) + x_h(t) + \Delta d(t) \tag{5}$$

where $x_b(t)$ and $x_h(t)$ represent the distance variation caused by heartbeat and breathing rhythms, and $\Delta d(t)$ denotes the residual signal. In addition, for short-range measurements (< 1.0 m), the residual phase noise $\Delta\theta(t)$ and the residual signal $\Delta d(t)$ can be neglected [25].

After receiving the processed signal, the measurement data are transmitted to a data acquisition system through a serial communication line for analog-to-digital conversion (ADC). In digital signal processing, a digital band-pass filter (Butterworth) is employed to remove the unwanted high- and low-frequency components. This way, we can obtain the heartbeat and breathing rhythm signals, $x_h(t)$ and $x_b(t)$. For the ECG signal sequence, FFT can be used to estimate the characteristic frequencies of signals, $x_b(t)$ and $x_h(t)$ [33, 34]. The peak detection algorithm was used to identify the R peaks within a QRS complex and thereby

TABLE 1 Specifications of the Doppler mm-wave radar [17].

Hardware	Specification
FMCW based transceiver	• 76–81 GHz Coverage with 4 GHz continuous bandwidth; • Four receive channels; • Two transmit channels; • Ultra-accurate chirp (timing) engine based on fractional-N PLL • Rx noise figure: 14 dB (76 to 77 GHz) / 15 dB (77 to 81 GHz)
DSP (Digital signal processor)	C674xDSP for FMCW signal processing
MCU (Microcontroller unit)	• ARM cortex-R4F microcontroller for application control • I/O: SPI / CAN × 1 • Up to 2 UARTs I2C × 1 (Raspberry Pi Hat Board [ARM® Cortex®-R4F-based radio control system])
Intend purpose	Vital signs detection (VSD) firmware for short-distance (30–90 cm) wireless and contactless detection for heart rate (HR) and respiration rate (RR) only one of VSD; HAM (pre-programmed within a single mmWave module)
Power consumption at power terminals	1.38–1.92 W for two transmitters and four receivers (25%–50% duty cycle, low power mode) [17]
Sensing range	0.6–1.2 m [5, 16, 29]
Operating temperature and humidity	• 0 to 40°C • 10%–85% non-condensing

extract the R-R interval parameters and compute the average HR. Table 1 presents the specifications of the contactless and short-range mm-wave sensors used in this study [5, 17, 29]. The proposed mm-wave radar does not require contact sensors or signal-conducting wires and can perform continuous, real-time VSD. In addition, the average power consumption of the W-band mm-wave sensor at the power terminals is approximately 1.38–1.92 W (25%–50% duty cycle), and the measurement distance is 0.6–1.2 m. Hence, the device is especially useful for application in patients with severe infectious diseases, serious and acute respiratory disorders, or burns in the ICU/NICU or isolation ward.

2.2 | HR and RR estimations

Human heartbeats and breathing rhythms are not fixed and are primarily regulated by the human autonomic nervous system. These heartbeats and breathing rhythms can be analysed using frequency- and time-domain methods to determine HR and RR. In both methods, the fragmented time-domain rhythm signals, as seen in approximately ten rhythm signals in Figures 3a and 4a, are used to estimate the HR and RR, respectively. In frequency-domain analysis, rhythm signals are transformed into a spectrogram by using the FFT method to identify the characteristic frequencies, as seen in Figures 3c and 4b, respectively. The HR and RR can be estimated by using the following equations:

$$\mathrm{HR} = 60 \times f_{c1}\ (\mathrm{beats/min}) \tag{6}$$

$$\mathrm{RR} = 60 \times f_{c2}\ (\mathrm{breaths/min}) \tag{7}$$

where f_{c1} is the characteristic frequency of the fragmented heartbeat signals; and f_{c2} is the characteristic frequency of the fragmented breathing rhythm signals, respectively. For adult subjects, the main frequency ranges within 1.1–1.3 Hz for heartbeats and frequency ranges between 0.15 and 0.40 Hz for breathing rhythm signals at stationary state. Lower frequency ranges, 0.04–0.15 Hz, reflect regulatory responses by the sympathetic and the parasympathetic systems.

In time-domain analysis, the R peak detection or endpoint detection algorithms [5, 6, 32] are used to extract the QRS complex wave in each heartbeat signal and then pick up the R peak, as seen in Figure 3a. Each R-R interval can be estimated between the R peak and the subsequent one, as displayed in Figure 3b. The average R-R interval is denoted as $R\text{-}R_{ave}$, which is used to estimate the average HR with the fragmented heartbeat signals (M heartbeats), as follows:

$$\mathrm{R-R_{ave}} = \frac{1}{\mathrm{M}} \sum_{\mathrm{m}=1}^{\mathrm{M}} \mathrm{R-R_m}\ (\mathrm{s}) \tag{8}$$

$$\mathrm{HR} = \frac{60}{\mathrm{R-R_{ave}}}\ (\mathrm{beats/min}) \tag{9}$$

Thus, Equations (6)–(9) can be employed to estimate the physiological parameters and indicators in real-time. Normal ranges of vital signs for adult humans are $48 < \mathrm{HR} < 120$ (beats/min) and $6 < \mathrm{RR} < 30$ (breaths/min), with slight variations based on factors such as age, sex, body weight, and health. These indices can assist in the early detection of life-threatening symptoms, such as coughing and shortness of breath, which are indicative of respiratory issues such as chronic obstructive pulmonary disease or acute respiratory distress syndrome (ARDS).

3 | EXPERIMENTAL RESULTS AND DISCUSSIONS

3.1 | Experimental setup

Experiments, tests, and validation of human VSD were conducted using the contactless mm-wave radar sensor, as seen in the sensing firmware in Figure 1a. The experimental HW setup employed a Doppler radar mm-wave sensing system [17], which included a 76–81 GHz (W-band) mm-wave sensing firmware (Joybien mm-Wave) with a Tx electromagnetic-wave transmitter and an Rx electromagnetic-wave receiver, a Raspberry-Pi Hat Board (ARM Cortex-R4F), an ADC, a microcontroller unit, and a digital signal heartbeats; (d) HR estimations with 30 heartbeats; (e) R-R interval estimations with 10, 20, and 30 heartbeats processor; and the HW-SW system was designed to carry out

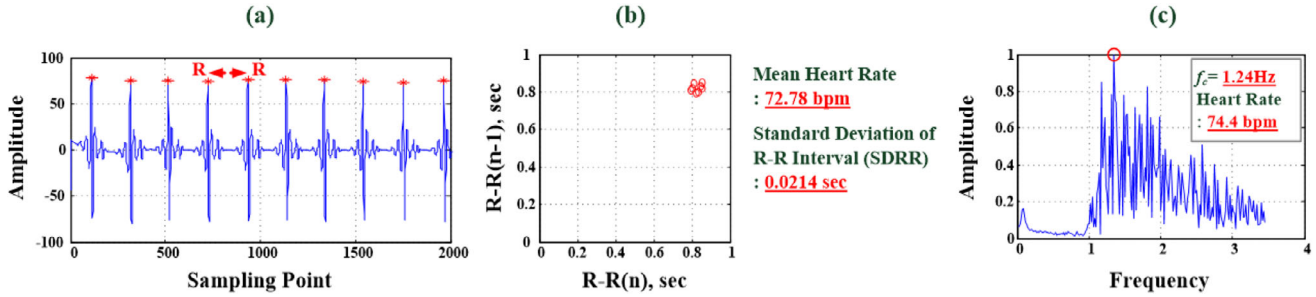

FIGURE 3 Time-domain and frequency-domain analysis for heartbeat signals. (a) Time-domain raw data for heartbeat signals. (b) Time-domain R-R interval analysis (HR = 72.78 bpm) and (c) frequency-domain HR analysis (f_{c1} = 1.24 Hz, HR = 74.4 bpm).

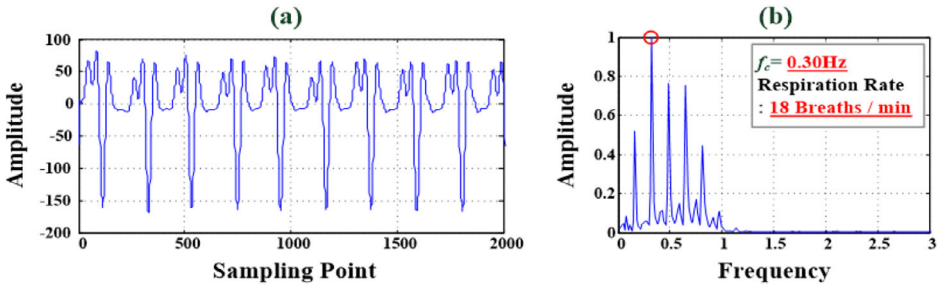

FIGURE 4 Time-domain and frequency-domain RR analysis for breathing rhythm signals. (a) Time-domain raw data for breathing rhythm signals. (b) Frequency-domain analysis for RR estimation (f_{c2} = 0.30 Hz, RR = 18 breaths/min).

the FMCW-based sensing functions for VSD at short range (0.30–1.20 m). The measurement distance was suggested at 0.6 m distance [5, 29]. The Raspberry-Pi Hat Board provided an integrated development environment, namely "Geany," for writing Python application programs. These programs are used to implement the mm-wave FMCW control, FFT operation, and time-domain analyses for processing the raw data. Hence, heartbeat and respiratory phase differences were processed with MATLAB 9.0 (MathWorks, Natick, MA, USA) version software and used to estimate HR and RR; these were then displayed on a graphical user interface (GUI). This system can also link to the internet of medical things (IOMT) systems via built-in Wi-Fi or Bluetooth wireless communication [35] for transmitting physiological measurements. This can be achieved through 2.4–2.485 GHz or 5.0–6.0 GHz ISM (Industrial, Science, and Medical, excluding applications in telecommunications) radio band standards (IEEE 802.11 Wireless Networking Protocol [36]). The 5G (fifth-generation) communication system [37] facilitates the transmission of a patient's data to remote hospitals or a clinician's smart phone and iPad, enabling hospitals, patients, and their families to monitor physiological parameters. This information can then be used in multiparty consultations and patient discussions for medical purposes.

3.2 | Experimental tests and discussion

The contactless VSD experiments and tests at 0.6 m distance (<1.0 m) were conducted in a laboratory, as shown in Figure 5a. Participants were ten young adult males with an average age of 22 years. Each participant underwent the stationary VSD test, recording heartbeats and breathing data for a 1-min timing interval for each measurement test. For instance, fragmented raw data from ten instances of heartbeats and breathing rhythms are portrayed in Figures 3a and 4a, respectively. Through time-domain analysis, the R-R interval was determined, and Equations (8) and (9) were employed to compute the average R-R interval and HR, respectively. As seen in Figure 3b, the average HR for the ten heartbeats depicted in Figure 3a was 72.78 beats/min (SDRR = 0.0214 s). The experimental results from the frequency-domain analysis are displayed in Figures 3c and 4b. The main characteristic frequencies, f_{c1} = 1.24 Hz and f_{c2} = 0.30 Hz, were extracted for ten instances of a heartbeat and breathing rhythm, where signified components of the measurement signals in the frequency ranges 0.8–2.0 and 0.1–0.6 Hz (frequency spectrum) were the cardiac and breathing signals, respectively. Equations (6) and (7) revealed that HR = 74.4 beats/min and RR = 18 breaths/min, respectively.

For fragmented raw data from 10, 20, and 30 instances of heartbeat signals, with frequency- and time-domain analysis, Figure 5b–d presented HRs for ten young participants at stationary VSD tests as average HRs of 71.66, 72.03, and 71.94 beats/min, respectively; and average R-R intervals of 0.8361, 0.8336, and 0.8345 s for time-domain analysis, respectively; and with ten participants' R-R intervals to compute HRs, Figure 5e shows the average HRs of 73.11, 74.06, and 73.68 beats/min for three fragmented raw data, respectively. All participants were healthy young adults, with their average HRs falling within the normal range of 48 beats/min < HR < 120 beats/min. It could be seen that the proposed mm-wave radar sensor had promising results for heartbeat measurement.

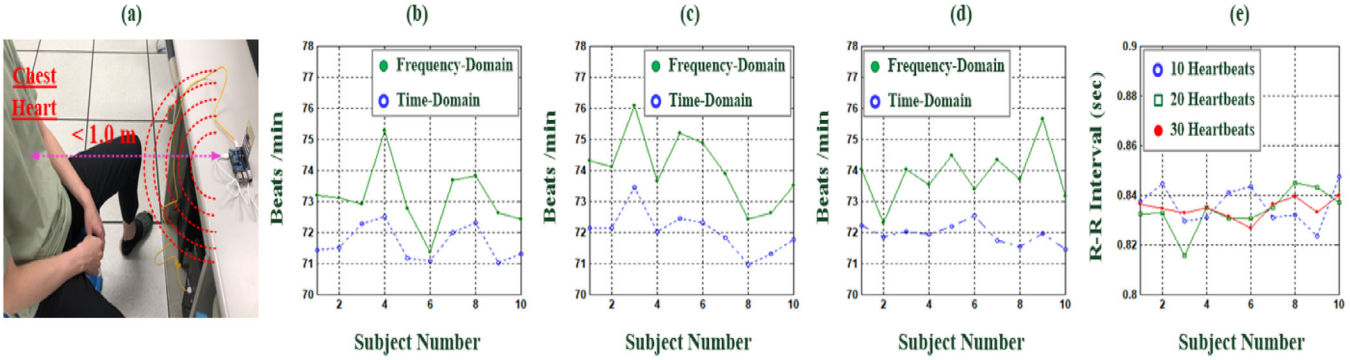

FIGURE 5 Experimental setup and frequency- and time-domain analysis for HR estimation with ten young adult subjects. (a) Experimental setup for VSD tests. (b) Frequency- and time-domain analysis for HR estimations with ten heartbeats. (c) HR estimations with 20.

TABLE 2 Comparisons of experimental results with different W-band mm-wave radarsensors.

Literature	HW-SW	Measurement distance	HR estimation	RR estimation
[5]	TI mm-wave radar sensor (IWR1443BOOST#), MATLab Application Software	0.3–1.5 m	67.12 beats/min (at a 0.6 m distance)	6–14 breaths/min (at a 0.6 m distance)
[29]	TI mm-wave radar sensor (IWR6843 and 1642BOOST#), MATLAB Application Software	0.6–1.0 m	76.00 beats/min (1.27 Hz, at a 1.0 m distance)	10.50 breaths/min (0.175 Hz at a 1.0 m distance)
Proposed Method	Joybien mm-wave radar sensor (TI IWR1642BOOST#), MATLAB and Python Application Software	0.6–1.0 m	72.02 beats/min (at a 0.6 m distance)	18.28 breaths/min (at a 0.6 m distance)

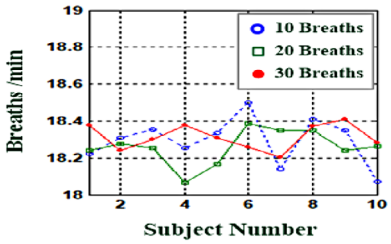

FIGURE 6 Frequency-domain analysis for RR estimations with 10, 20, and 30 breaths (ten young adult subjects).

Figure 6 presents the frequency-domain RR estimations for the 10, 20, and 30 breathing rhythm signals of the ten young adult participants. The average RRs were 18.29, 18.26, and 18.31 breaths/min, respectively, within the normal RR range of 6–30 breaths/min. To investigate the contactless performance of the method, 1-min stationary VSD tests at a distance of 0.6 or 1.0 m were performed using the proposed method (TI IWR6843BOOST) and W-band mm-wave radar sensors described in the literature (TI IWR1443 and TI IWR1642 BOOST) [5, 29]. The experimental results are presented in Table 2. The proposed mm-wave system obtained promising results for both HR and RR estimation at 0.6 m. A comparison of the results of our mm-wave radar system with those of ECG and PPG detection is presented in Table 3. ECG measurements capture weak voltage signals through active or passive electrodes on the skin. The ECG sensing circuit must contain high-gain analog and digital high-pass (Butterworth) filters, band-rejection filters, and baseline-drift filters to remove noise due to interference from power circuits (50 and 60 Hz), electromagnetism, and skin contact impedance. These contact sensing and filtering circuits can readily be integrated into a wearable device. In clinical applications, 12-lead measurements can also be used to obtain ECG signals from limb and chest leads. Continuous monitoring of cardiac electrical activity signals through conventional ECG limits patient movement, and the measurement quality is easily degraded.

Additionally, PPG measurement employed the single- or dual-wavelength light sources (650 nm or 800–940 nm) to measure pulse signals and oxygen saturation in the transmissive or reflective modes [1, 3, 4, 7]. Although reflective mode can be used on any part of the body, the use of an optical detector, which detects a change in the light flux at different depths, means that the reflected signal has to undergo further processing, such as noise filtering, signal amplification, signal modulation, and signal digitization. Commercial optical sensors are compact and lightweight; photoemitters, photoreceivers, and driver circuits can be easily integrated into an embedded system to suppress ambient light, reduce power consumption, and extend the possible monitoring duration. In clinical applications, combining ECG and PPG measurements can be effective for detecting peripheral arterial disease through the assessment of a patient's arteriosclerosis risk level [4, 38]. The R peak can be used as a timing reference, as seen in Figure 7a,b, enabling the extraction of specific pulse feature parameters

TABLE 3 Comparisons of mm-wave radar sensor, ECG, and PPG detection.

VSD methods	Millimetre (Mm)-wave radar	ECG measurement	PPG measurement
Principles (technology)	Doppler radar detection of millimetre waves	Detection of physiological signals from the heart through electrodes on the skin	Optical detection of pulse signals through direct contact with the skin
Detection signals	76–81 GHz electromagnetic waves (incident and reflected electromagnetic waves)	Heart nerve conduction signals (changes in cardiomyocyte depolarization voltages)	Infrared light (650 nm) or near-infrared light (800–940 nm) [1, 3, 4, 7]
Detection approach	Contactless Sensing	Contact Sensing	Contactless/Contact Sensing
Detection distance	Short-range (0.3–1.2 m) [5, 29]	Active or passive detection through electrodes on skin	Transmissive and reflective light sensors on the skin
Wearable	×	√	√
Sources of interference and noise	Uses short-wavelength mm-wave and short-range measurement to avoid unnecessary environmental noise (slight)	Power harmonic interference (50 Hz/60 Hz), skin contact impedance interference, electromagnetic interference, interference caused by human vibrations	Interference from ambient light (fluorescent lights and energy-saving lamps), sweat, and motion vibrations
Filter requirement	√	√	√
Monitoring type	Continuous monitoring	Continuous monitoring	Continuous monitoring
Movement restrictions	×	√	√
Medical purpose (applications)	HR and RR estimation	• HR and RR estimation • Sympathetic nerve activity evaluation • Temperature regulation response evaluation • Peripheral cardiovascular tone and reflex evaluation	• HR and RR estimation • SPO_2 estimation • Blood flow velocity estimation • Stiffness index (SI) estimation • Reflection index (RI) estimation

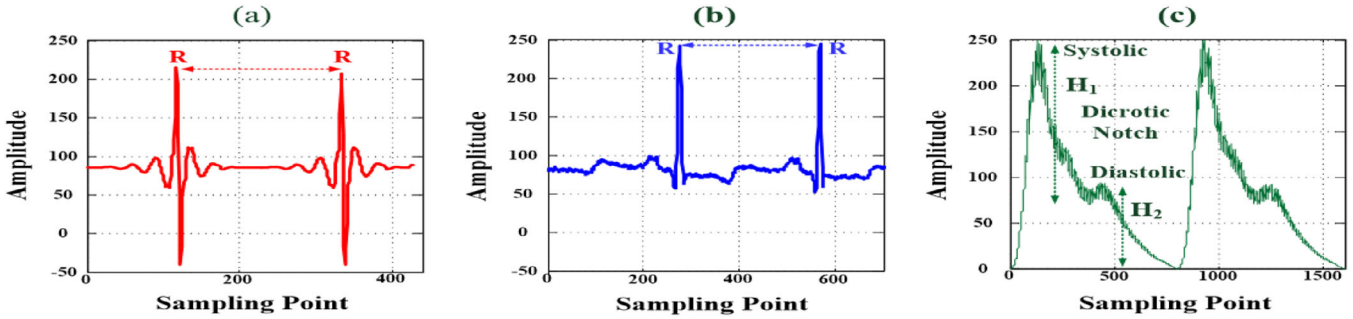

FIGURE 7 ECG and PPG signals of vital signs: (a) millimetre-wave radar detection of ECG signals; (b) lead II detection of ECG signals; and (c) infrared photoreceiver detection of PPG signals.

from the time-domain PPG waveforms, such as differences in the pulse transit time between the ECG R peak and the PPG foot, timing intervals between pulse waves, and peak height ratios of the pulse signals. These parameters can be used to measure the SI and RI [1, 3, 4, 7, 39], for example, $RI = (H_2 / H_1) \times 100\%$, as seen in Figure 7c. Hence, the 76–81 GHz mm-wave radar sensor developed in this study offers several advantages compared to ECG and PPG measurements:

- It enables contactless and short-range sensing manner.
- It offers suitable directionality from the mm-wave antenna emitting electromagnetic waves, which aids in controlling the sensing range.
- It bears a strong resistance to interference from environmental factors such as temperature, humidity, noise, airflow, dust, and light.
- It exhibits a high level of resistance to radio frequency interference.
- It produces low output power that is harmless to humans.

Figure 7a,b shows the raw data from the mm-wave radar and a lead II ECG in the time domain, respectively. Both waveforms had distinct and periodic R peaks and could be used to estimate the R-R interval. In combination with the fragmented heartbeat signals, the average HR could be easily calculated using Equations (8) and (9). In this study, the developed mm-wave radar

sensing method achieved contactless and short-range heartbeat signal detection. Numerous ECG and PPG measurements were performed to gather raw data that was used to evaluate patient risk for peripheral arterial disease, cardiac arrhythmia, and arteriosclerosis, as well as sympathetic nervous system activity and temperature regulation responses. ECG waveforms have been used to identify cardiac arrhythmia types, heart conduction abnormalities, coronary ischemia, and atrial fibrillation based on the detected P wave, QRS complex wave, and T wave. Future studies should aim to acquire more heartbeat signals from patients with cardiovascular diseases to validate the applicability of the 76–81 GHz mm-wave radar sensor for VSD and disease examination.

4 | CONCLUSION

In-hospital and at-home IOMT systems with sensors enable the collection and transmission of vital sign data. Such systems can be used for the continuous collection of medical data, including heartbeat and breathing signals, blood pressure, and other biochemical examination data. Physiological signals can be obtained using the proposed contactless and short-range sensor and then analysed in the time and frequency domains to assist in the early detection of the symptoms of cardiopulmonary diseases. In this study, VSD experiments involving a group of healthy young adults were conducted using a 76–81 GHz mm-wave radar sensor at a distance of 0.6 m. The system yielded promising results for HR and RR estimations, demonstrating its feasibility for contactless detection. VSD is a critical tool for patient monitoring, particularly in patients with infectious respiratory diseases such as COVID-19, those in ICUs and NICUs, and those in isolation wards. Contactless methods can reduce human -to-human transmission and improve infectious disease control. The proposed mm-wave radar sensor can facilitate continuous vital sign monitoring. Moreover, it can be integrated with 5G communication technologies to simplify the processing of the data collected by IOMT systems. Collected data can be analyzed and features extracted before they are ultimately used in artificial intelligence (AI)-based diagnosis methods, such as machine learning (ML) and deep learning (DL)-based diagnostic algorithms. In summary, this study demonstrated the feasibility of the proposed mm-wave radar for contactless VSD. The tool can be applied in future clinical applications to monitor heartbeat signals related to atrial fibrillation, supraventricular tachycardia, ventricular tachycardia, and bundle branch block beat and thereby contribute to AI classification. The combination of the mm-wave radar sensor with an AI-based classifier would be considered a Class II medical device; before licensing and approval of this device, its electrical safety, effectiveness, accuracy, and risk must be evaluated (IEC60601 [40]), and clinical testing and validation must be performed. It could then be integrated into an IOMT system.

AUTHOR CONTRIBUTIONS

Pi-Yun Chen: Project administration; conceptualization; methodology. **Hsu-Yung Lin**: Investigation; data curation. **Zi-Heng Zhong**: Investigation; data curation. **Neng-Sheng Pai**: Methodology; formal analysis. **Chien-Ming Li**: Investigation; conceptualization. **Chia-Hung Lin**: Investigation; methodology; formal analysis.

CONFLICT OF INTEREST STATEMENT

The authors declare no conflicts of interest.

DATA AVAILABILITY STATEMENT

Data available on reasonable request from the authors.

ORCID

Chia-Hung Lin https://orcid.org/0000-0003-0150-8001

REFERENCES

1. Allen, J.: Photoplethysmography and its application in clinical physiological measurement. Physiol. Meas. 28(3), R1–R39 (2007)
2. Villarroel, M., Guazzi, A., Jorge, J., Davis, S., Watkinson, P., Green, G., Shenvi, A., McCormick, K., Tarassenko, L.: Continuous non-contact vital sign monitoring in neonatal intensive care unit. Healthcare Technol. Lett. 1(3), 87–91 (2014)
3. Kyriacou, P., Allen, J.: Photoplethysmographyechnology, Signal Analysis and Applications, 1st ed. Academic Press, Cambridge, MA (2021)
4. Wu, J.-X., Lin, C.-H., Kan, C.-D., Chen, W.-L.: Bilateral photoplethysmography for peripheral arterial disease screening in hemodialysis patients using astable multi-vibrator and machine learning classifier. IET Sci. Meas. Technol. 13(9), 1277–1286 (2019)
5. Iyer, S., Zhao, L., Mohan, M.P., Jimeno, J., Siyal, M.Y., Alphones, A., Karim, M.F.: mm-Wave radar-based vital signs monitoring and arrhythmia detection using machine learning. Sensors 22(9), 1–20 (2022)
6. Lin, C.-H., Wu, J.-X., Chen, P.-Y., Li, C.-M., Pai, N.-S., Kuo, C.-L.: Symmetric cryptography with a chaotic map and a multilayer machine learning network for physiological signal infosecurity: Case study in electrocardiagram. IEEE Access 9, 26451–26467 (2021)
7. Lin, C.-H., Wu, J.-X., Pai, N.-S., Chen, P.-Y., Li, C.-M., Pai, C.C.: Intelligent physiological signal infosecurity: Case study in photoplethysmography (PPG) signal. IET Signal Proc. 16(3), 267–280 (2022)
8. Sharkey, E.J., Maria, C.D., Klinge, A., Murray, A., Zheng, D., O'Sullivan, J., Allen, J.: Innovative multi-site photoplethysmography measurement and analysis demonstrating increased arterial stiffness in paediatric heart transplant recipients. Physiol. Meas. 39(7), 074007 (2018)
9. Li, Q., Rajagopalan, C., Clifford, G.D.: Ventricular fibrillation and tachycardia classification using a machine learning approach. IEEE Trans. Biomed. Eng. 61(6), 1607–1613 (2014)
10. Das, M.K., Ari, S.: Patient-specific ECG beat classification technique. Healthcare Technol. Lett. 1(3), 98–103 (2014)
11. Lazim, M.R.M.L.M., Aminuddin, A., Chellappan, K., Ugusman, A., Hamid, A.A., Ahmad, W.A.N.W., Mohamad, M.S.F.: Is heart rate a confounding factor for photoplethysmography markers? A systematic review. Int. J. Environ. Res. Public Health 17, 1–12 (2020)
12. Allen, J., Overbeck, K., Nath, A.F., Murray, A., Stansby, G.: A prospective comparison of bilateral photoplethysmography versus the ankle-brachial pressure index for detecting and quantifying lower limb peripheral arterial disease. J. Vasc. Surg. 47(4), 794–802 (2008)
13. Sharkey, E.J., Maria, C.D., Klinge, A., Murray, A., Zheng, D., O'Sullivan, J., Allen, J.: Innovative multi-site photoplethysmography measurement and analysis demonstrating increased arterial stiffness in paediatric heart transplant recipients. Physiol. Meas. 39(7), 074007 (2018)
14. Jin, H., Yang, S., Yang, F., Zhang, L., Weng, H., Liu, S., Fan, F., Li, H., Zheng, X., Yang, H., Zhang, Y., Zhou, J., Li, J.: Elevated resting heart rates are a risk factor for mortality among patients with coronavirus disease 2019 in Wuhan, China. J. Transl. Int. Med. 9(4), 285–293 (2021)
15. da Silva, A.C.R., Juliana, F., Sidrônio, C.D., do Rêgo, B.A.E.V., Ferreira, S.J.A., da Glória Rodrigues, M.M., Aguiar, Remígio, M.I., Soares, B.S.C., Lima, C.S., de Fatima Dornelas, A.A., Cunha, B.D.: Endothelial function,

arterial stiffness and heart rate variability of patients with cardiovascular diseases hospitalized due to COVID-19. Heart Lung 58, 210–216 (2023)
16. Song, Y., Fang, J., Zhang, K., Su, R., Zhang, N., Zhao, Y.: Multi-state FMCW radar real-time vital signs monitoring system. In: Proceedings of the 2023 IEEE 6th International Conference on Electronic Information and Communication Technology (ICEICT), Qingdao, China, pp. 205–210. IEEE, Piscataway, NJ (2023)
17. Joybien Technologies Co, Ltd.: Joybien mmWave, 2023Years. https://computer-consultant-1700.business.site/ and https://www.joybien.com/. Accessed January, 2024
18. Dekker, B., Jacobs, S., Kossen, A.S., Kruithof, M.C., Huizing, A.G., Geurts, M.: Gesture recognition with a low power FMCW radar and a deep convolutional neural network. In: Proceedings of the 2017 European Radar Conference, pp. 163–166. IEEE, Piscataway, NJ (2017)
19. Peng, B., Liu, Z., Wei, X., Li, X.: Sinusoidal frequency modulation sparse recovery for precession rate estimation using low-frequency long-range radar. IEEE Sens. J. 15(12), 7329–7340 (2015)
20. Lin, C.-H., Wu, J.-X., Hsu, J.-C., Chen, P.-Y., Pai, N.-S., Lai, H.-Y.: Tremor class scaling for ennessee disease patients using an array X-band microwave Doppler based upper limb movement quantizer. IEEE Sens. J. 21(19), 21473–21485 (2021)
21. IEEE Aerospace and Electronic Systems Society: IEEE Standard 686–2017 for radar definitions, IEEE Std 686–2017. IEEE, Piscataway, NJ (2017)
22. Jung, D., Cheon, S., Kim, D., Yoon, J., Kim, B.: Short time remote heart rate measurement based on mmWave FMCW radar frame structure. IEEE Antennas Wirel. Propag. Lett. 14(8), 1–5 (2021)
23. Zongquan, L., Zhou, W., Ren, Y., Wang, J., Guo, L.: Non-contact heart rate monitoring based on millimeter wave radar. IEEE Access 10, 74033–74044 (2022)
24. Wang, F., Zeng, X., Wu, C., Wang, B., Ray Liu, K.J.: Driver vital signs monitoring using millimeter wave radio. IEEE IoT J. 9(13), 11283–11298 (2022)
25. Wang, F., Zhang, F., Wu, C., Wang, B., Ray Liu, K.J.: ViMo: multiperson vital sign monitoring using commodity millimeter-wave radio. IEEE IoT J. 8(3), 1294–1307 (2021)
26. Berlo, B., Elkelany, A., Ozcelebi, T., Meratnia, N.: Millimeter wave sensing: a review of application pipelines and building blocks. IEEE Sens. J. 21(9), 10332–10368 (2021)
27. Shafiq, G., Veluvolu, K.C.: Surface chest motion decomposition for cardiovascular monitoring. Sci. Rep. 4, 1–9 (2014)
28. Shyu, K.-K., Chiu, L.-J., Lee, P.-L., Lee, L.-H.: UWB simultaneous breathing and heart rate detections in driving scenario using multi-feature alignment two-layer EEMD method. IEEE Sens. J. 20(17), 10251–10266 (2020)
29. Oleksak, K.: Vital sign detection using millimeter wave radars. Master Thesis, University of Tennessee (2020). https://trace.ennessee.edu/utk_gradthes/5609
30. Zhang, J., Xi, R., He, Y., Sun, Y., Guo, X., Wang, W., Na, X., Liu, Y., Shi, Z., Gu, T.: A survey of mmWave-based human sensing: technology, platforms and Applications. IEEE Commun. Surv. Tutor. 25(4), 2052–2087 (2023)
31. Akselrod, S., Gordon, D., Ubel, F.A., Shannon, D.C., Berger, A.C., Cohen, R.J.: Power spectrum analysis of heart rate fluctuation: a quantitative probe of beat-to-beat cardiovascular control. Science 213(4504), 220–222 (1981)
32. Wu, J., Chong, G., Pang, W., Wang, L.: Speech endpoint detection based on EMD and improved spectral subtraction. In: Proceedings of the 2023 5th International Conference on Natural Language Processing (ICNLP), pp. 126–130. IEEE, Piscataway, NJ (2023)
33. Garde, A., Karlen, W., Dehkordi, P., Ansermino, J., Dumont, G.: Empirical mode decomposition for respiratory and heart rate estimation from the photoplethysmogram. Comput. Cardiol. 40, 799–802 (2013)
34. Prathyusha, B., Rao, T.S., Asha, D.: Extraction of respiratory rate from PPG signals using PCA and EMD. Int. J. Res. Eng. Technol. 1(2), 164–184 (2012).
35. Ghubaish, A., Salman, T., Zolanvari, M., Unal, D., Al-Ali, A., Jain, R.: Recent advances in the internet- of- medical-things (IoMT) systems security. IEEE IoT J. 8(11), 8707–8718 (2021)
36. The Working Group for WLAN Standards: IEEE 802.11TM wireless local area networks. https://www.ieee802.Org/11/. Accessed January, 2024
37. Kamal, M.M., Yang, S., Kiani, S.H., Anjum, M.R., Alibakhshikenari, M., Arain, Z.A., Jamali, A.A., Lalbakhsh, A., Limiti, E.: Donut-shaped mmwave printed antenna array for 5G technology. Electronics 10(12), 1–10 (2021)
38. Wu, J.-X., Li, C.-M., Ho, Y.-R., Wu, M.-J., Huang, P.-T., Lin, C.-H.: Bilateral photoplethysmography analysis for peripheral arterial stenosis screening with a fractional-order integrator and info-gap decision-making. IEEE Sens. J. 16(8), 2691–2700 (2016)
39. Velzen, M.H.N., Loeve, A.J., Niehof, S.P., Mik, E.G.: Increasing accuracy of pulse transit time measurements by automated elimination of distorted photoplethysmography waves. Med. Biol. Eng. Comput. 55(11), 1989–2000 (2017)
40. IEC 60601-1:2023 SER Series: Medical electrical equipment, 2023 years. https://webstore.iec.ch/publication/2603. Accessed January, 2024

How to cite this article: Chen, P.-Y., Lin, H.-Y., Zhong, Z.-H., Pai, N.-S., Li, C.-M., Lin, C.-H.: Contactless and short-range vital signs detection with doppler radar millimetre-wave (76–81 GHz) sensing firmware. Healthc. Technol. Lett. 11, 427–436 (2024). https://doi.org/10.1049/htl2.12075